



Scattering spot imaging for the determination of optical and dynamical properties of viscoelastic media

Christelle Abou Nader, Jean-Michel Tualle^{*}, Eric Tinet, Dominique Ettori

Laboratoire de Physique des Lasers, CNRS UMR 7538, Institut Galilée, Université Paris 13, 99 Av. J. B. Clément, F-93430 Villetaneuse, France

ARTICLE INFO

Keywords:

Speckle
Correlation spectroscopy
Dynamical properties
Optical properties

ABSTRACT

The non-contact evaluation of dynamical properties of media presents several medical, biological, and industrial applications. Diverse optical methods, operating at different scales with various targeted applications, are currently being considered as alternatives to traditional mechanical testing devices. However, the accuracy of most optical techniques upon multiple scattering is compromised by the influence of the medium's optical properties, namely scattering and absorption. Therefore, in order to accurately estimate dynamical properties, that are related to mechanical features, it is of pivotal importance to determine the medium's optical properties. In this paper, we present a new simple scheme for the assessment of optical as well as dynamical properties of viscoelastic media. We demonstrate, for the first time, the possibility of estimating absorption, scattering, and dynamical properties using scattering spot imaging with a standard CCD camera at multiple exposure times and with a monochromatic continuous wave (CW) illuminance.

1. Introduction

Viscoelasticity is the property of materials displaying both viscous and elastic characteristics when undergoing deformation. Various media such as synthetic polymers, fruits, vegetables, and human tissue exhibit viscoelastic behavior. In many fields, such as tissue engineering, medical diagnosis, and food processing and handling [1–3], the assessment of mechanical properties of media can be beneficial for a variety of purposes. Mechanical properties of materials are conventionally evaluated using mechanical testing systems, by stretching or applying a compression to the sample. The relationship between the deformation and the applied shear stress is expressed through the viscoelastic modulus $G^*(\omega)$. These methods include tensile testing, compression testing, micro- and nano-indentation, and magnetic force techniques. However, depending on the sample's nature, the measurement of its viscoelastic properties in a non-destructive manner could be beneficial or even essential. Numerous techniques such as ultrasound [4] are currently being tested for non-destructive measurements. Optical methods, targeting different applications, are also being tested and considered to replace traditional mechanical procedures [5–7]. These optical techniques could potentially offer the advantage of performing non-destructive, non-contact, non-invasive, or less time-consuming measurements [8–11].

The analysis of the speckle pattern is an emerging approach for the investigation of optical properties of media on one hand [12], and their dynamical features, reflecting their mechanical properties, on the other hand. Previous studies have proven the ability of the speckle contrast to determine the diffusion properties of strongly scattering thin slabs based

on a speckle contrast measurement and illumination with a femtosecond laser of variable spectral bandwidth [13]. Viscous and elastic properties of fluids and tissues were also estimated using speckle contrast and speckle temporal correlations [14–16]. In fact, in a viscoelastic medium, the strain could be measured through changes in scattering particles positions reflected by their mean square displacement (MSD). Previous studies have proven that the MSD is related to the sample's mechanical properties, namely the viscoelastic modulus $G^*(\omega)$, via the generalized form of the Stokes–Einstein equation [17–19].

The theories that are classically used in order to extract the MSD from speckle temporal correlation measurements are: Dynamical Light Scattering (DLS) for single scattering [20,21] and Diffusing Wave Spectroscopy (DWS) for strong multiple scattering [22]. Another approach to study speckle correlations is the correlation diffusion theory [23,24]. It is frequently used for biomedical applications, such as the monitoring of blood flow [25–27]. In the case of poorly scattering media, having low scattering coefficients, the extraction of the MSD is a straightforward task. However, for highly scattering samples, it is imperative to determine the optical properties before trying to extract any dynamical information.

In this work, we present a novel method for the simultaneous evaluation of both optical and dynamical properties of viscoelastic materials. It is based on speckle contrast and intensity profile measurements of the scattering spot observed in transillumination through a sample slab, with a monochromatic CW illumination, and for different exposure times. We show, for the first time, that the absorption and

^{*} Corresponding author.

E-mail address: tualle@univ-paris13.fr (J.-M. Tualle).

reduced scattering coefficients, as well as dynamical parameters, can be extracted using an inverse Monte Carlo algorithm based on the diffusion correlation theory. The capacity of the proposed approach is tested on speckle images of virtual media, with known optical and dynamical properties, generated using a Monte Carlo algorithm. All parameters were retrieved with an average accuracy of 3%, and a maximum discrepancy of 24%. Furthermore, to prove the applicability of our approach on real biological media, we show experiments conducted on apple slices for which we estimate scattering, absorption and dynamical properties.

2. Materials and methods

2.1. Theoretical background

According to the correlation diffusion theory, the electric field temporal autocorrelation function $G_1(\vec{r}, \tau) = \langle E(\vec{r}, t) E^*(\vec{r}, t + \tau) \rangle$, which depends on the position \vec{r} and on the correlation time τ , propagates like the light fluence rate, but with an additional absorption term $\mu(\tau)$. This term $\mu(\tau)$ can be understood as a kind of “correlation absorption” due to the dynamics of the medium, and is added to the standard absorption coefficient μ_a . Introducing the reduced scattering coefficient $\mu'_s = (1 - g)\mu_s$, where μ_s is the scattering coefficient and g is the anisotropy factor, one has [25]: $\mu(\tau) = \mu'_s k^2 \langle \Delta r^2(\tau) \rangle / 3$ where k is the wave number, and $\langle \Delta r^2(\tau) \rangle$ is the MSD of the medium’s scattering centers during time τ . We consider an infinite homogeneous slab with a thickness z , a circular 2 mm diameter source, a transmission collection geometry and, assuming a cylindrical symmetry, a separation r along the sample’s output face between the scattering spot center and the observation point.

The speckle contrast $C(r, T_{\text{exp}})$ is defined as the ratio of the standard deviation σ of the recorded speckle pattern to its mean intensity I : $C(r, T_{\text{exp}}) = \sigma(r, T_{\text{exp}}) / I(r, T_{\text{exp}})$. It can be computed as a function of $G_1(r, \tau)$ and the exposure time T_{exp} as follows [28] (see Appendix for a complete derivation):

$$C(r, T_{\text{exp}}) = \frac{1}{T_{\text{exp}}} \sqrt{2\beta \int_0^{T_{\text{exp}}} (T_{\text{exp}} - \tau) \frac{G_1^2(r, \tau)}{G_1^2(r, 0)} d\tau} \quad (1)$$

$C(r, T_{\text{exp}})$ is in fact a temporal contrast that depends on the radial coordinate r due to the fact that laterally scattered light undertakes more scattering events as r increases, and thus induces faster decorrelation times. The parameter β introduced in this expression accounts for a reduction in contrast associated to experimental conditions such as polarization and mismatch between the camera pixels and the speckle size. Therefore, Eq. (1) allows the computation of the speckle contrast from any light transport model once the optical properties and the MSD of the medium are known.

The MSD takes different forms for free diffusion, confined diffusion, anomalous diffusion, and flow or directed motion. Usually, for complex media, the MSD can be expressed as linear combinations of these forms for different diffusion regimes [29]. In this work, we choose to focus on viscoelastic hydrated tissue-like media composed of two types of scattering centers: freely diffusing spheres, and confined ones, both immersed in a viscous fluid. Therefore, the MSD can be expressed as follows [30]: $\text{MSD} = \langle \Delta r^2(\tau) \rangle = r_0^2 \left(1 - e^{-\frac{\tau}{\tau_D}} \right) + 6D_F \tau$, where r_0 is the radius within which the particle is confined, τ_D is the diffusion time constant of the confined scatterers, and D_F is the diffusion constant of the freely diffusing scatterers.

2.2. Methodology and numerical simulation

For a medium of definite thickness, illuminated with a known wavelength, the contrast C at different r positions, acquired at a certain exposure time T_{exp} , will depend on: μ_a , μ'_s , r_0 , τ_D , and D_F . The dependence of the speckle contrast on all these 5 parameters is nontrivial, and

it is therefore a great challenge to get information on these parameters from contrast measurements only, even with variations of the latter over the exposure time and over the separation radius r . In order to overcome this issue, we also consider the intensity profile $I(r)$.

The estimation of the 5 parameters of interest, i.e. μ_a , μ'_s , r_0 , τ_D , and D_F becomes subsequently possible by applying an inverse Monte Carlo fitting algorithm on $I(r)$ and $C(r, T_{\text{exp}})$. We chose to use the Monte Carlo method, instead of the diffusion approximation, for the evaluation of $G_1(r, \tau)$ in order to avoid discrepancies that might be introduced by this approximation. Nevertheless, we are not far from the diffusion regime, so the introduction of μ'_s is still relevant, with a crude approximation for g and for the phase function in order to implement the numerical simulation. In the following, we take $g = 0.8$, with a Henyey–Greenstein phase function [31] and with more than 1 billion photons for each simulation.

In order to fit both $I(r)$ and $C(r, T_{\text{exp}})$, we propose the following method: after setting different tissue-relevant μ_a values (from 0.01 to 1 cm^{-1}), the μ'_s is returned for each μ_a by applying the fit to the intensity profile $I(r)$, yielding an error $E_I(\mu_a)$. These estimated values of μ_a and μ'_s are then used as fixed parameters while fitting $C(r, T_{\text{exp}})$ curves. Subsequently, r_0 , τ_D , and D_F are extracted with an error value $E_C(\mu_a)$. Two distinct sets of parameters, corresponding to the minimum error values, $E_{C,\text{min}}$ and $E_{I,\text{min}}$, are the ones extracted and assessed. Note that the retrieval of the parameters of interest from the performed adjustments is done using the Nelder–Mead simplex method, starting from the expected magnitudes for the different parameters ($\mu'_s = 5 \text{ cm}^{-1}$, $r_0 = 10^{-6} \text{ cm}$, $\tau_D = 5 \text{ ms}$ and $D_F = 10^{-14} \text{ cm}^2 \text{ ms}^{-1}$).

This approach is applied on Speckle images of virtual tissue-mimicking media with known optical and dynamical properties in order to test its accuracy in estimating all 5 parameters of interest. Simulated speckle images under different T_{exp} values ranging from 0.5 to 95 ms are generated using Monte Carlo simulations. We exploit here specific simulation runs, completely decorrelated with the simulations used for the fit, in order to avoid bias from noise patterns correlations. From these simulations, we get values for $I(r)$ and $C(r, T_{\text{exp}})$, and we generate random images with an exponential added noise, having an average $I(r)$ and standard deviation $\sigma = C(r, T_{\text{exp}}) I(r)$. The dynamical aspect is taken into account from Eq. (1) by adding the $\mu(\tau)$ factor discussed previously in order to compute $G_1(r, \tau)$. This is done in Monte Carlo simulations using the Beer–Lambert law, with an $\exp[-\mu(\tau)l]$ factor for trajectories of length l . Let us underline the fact that, as the speckle noise is the main source of noise in such experiments, those simulations are representative of the experimental reality. In the algorithm, we consider a transillumination geometry through a slab of thickness $z = 1.2 \text{ cm}$, a CW illumination (wavelength $\lambda = 780 \text{ nm}$), a source diameter of 2 mm, and a refractive index $n = 1.4$. The parameter β is fixed to the value $\beta = 0.54^2$ obtained from experimental measurements.

The proposed methodology is illustrated in Fig. 1. On the speckle images, the scattering spot center is detected (step 1) using an algorithm that searches for circular patterns and extracts the average intensity as a function of the distance r from the center. The contrast is also computed over multiple rings with the same center as the scattering spot, with a width of 0.04 cm, and for different values for their radius (0.8, 0.9, 1 and 1.1 cm). Note that for small radii ($r < 0.8 \text{ cm}$), the behavior of the contrast is very similar to the one corresponding to $r = 0.8 \text{ cm}$. However, for such radii, the integration rings have smaller surfaces. Consequently, we consider rings at radii starting from 0.8 cm where we have a high signal to noise ratio, and where the contrast starts having an interesting behavior as a function of the radius r . Step 2 of Fig. 1 shows an example of the calculated $I(r)$ and $C(r, T_{\text{exp}})$, on which we perform the fitting process. With increasing r positions, a faster decay of C is observed versus T_{exp} . This behavior is typical, and is due to the fact that for longer path lengths, meaning at larger distances away from the scattering spot, the photons would have undergone more scattering events, leading to a lower contrast. Step 3 consists on fitting the intensity profile as a function of μ_a in order to get an optimal value of μ'_s for

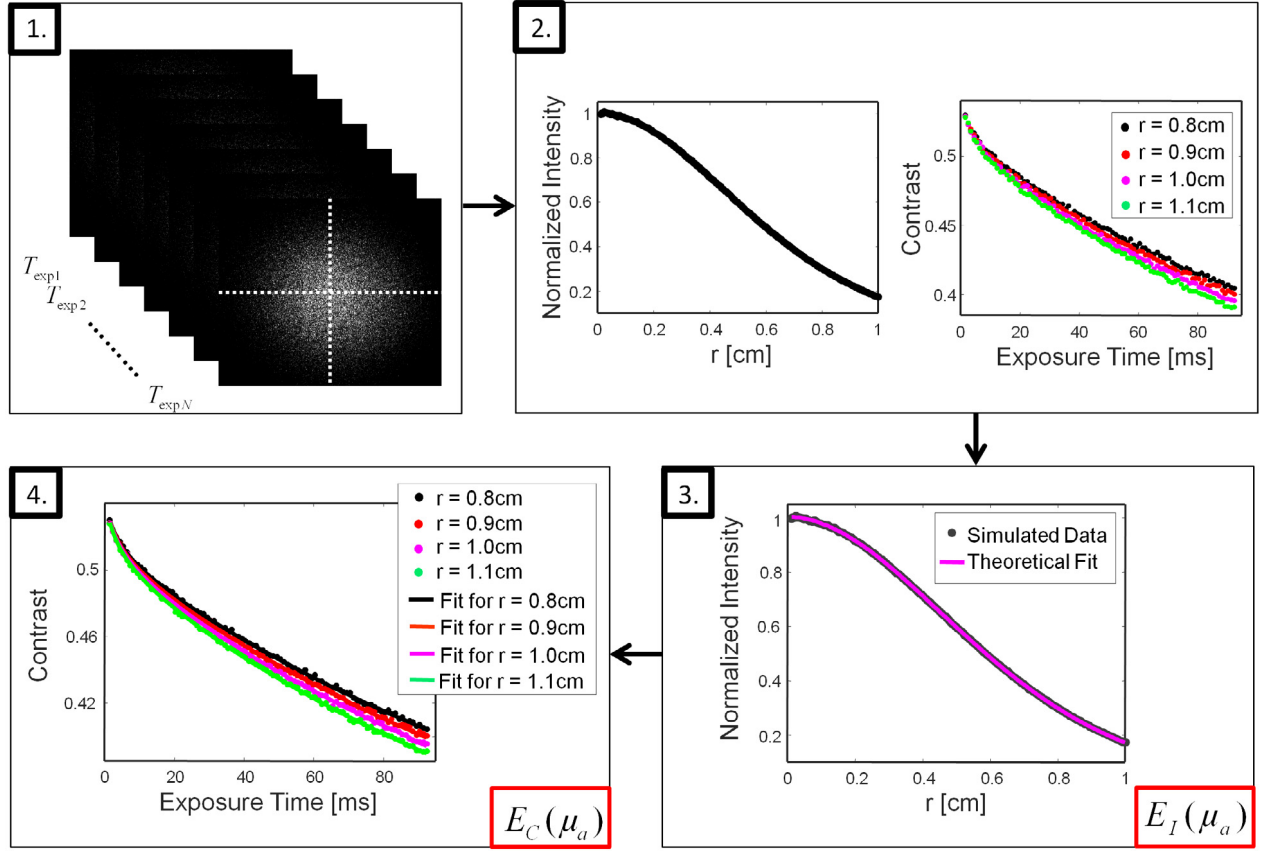


Fig. 1. Detailed chart of the proposed methodology. With increasing r positions, a faster decay of the contrast is observed versus the exposure time. Step 1: Detect the center of the scattering spot on speckle images acquired at different exposure times. Step 2: Calculate intensity and contrast profiles. Step 3: Fit the normalized intensity for different μ_a values to get $\mu'_s(\mu_a)$. Step 4: Fit the contrast for the values of μ_a and $\mu'_s(\mu_a)$ given by step 3 to get τ_0 , τ_D and D_F .

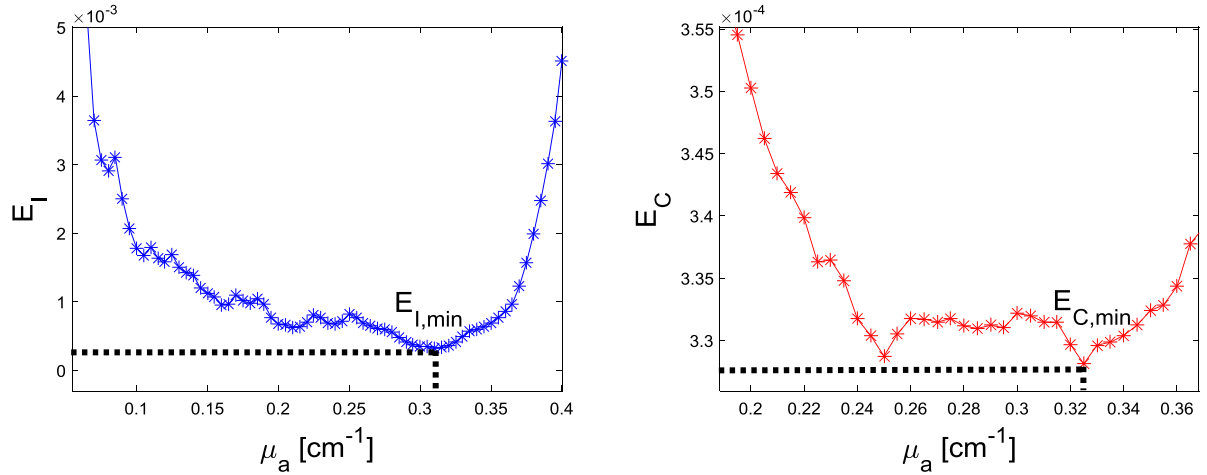


Fig. 2. E_I and E_C corresponding to the errors between the fit and the simulated intensity and contrast profiles (respectively) as a function of the set μ_a value. $E_{I,min}$ and $E_{C,min}$ are the values corresponding to the minimum of E_I and E_C and are marked with the dotted line on each graph.

each μ_a . This procedure yields an error $E_I(\mu_a)$ corresponding to the discrepancy between the intensity profile and its fit (*i.e.* to the sum of the squared residuals between actual values of intensity and their fitted values). The value of μ'_s is then fixed for each μ_a , and the contrast profiles are fitted for each pair $(\mu_a; \mu'_s)$, which provides the three dynamical parameters (τ_0 , τ_D , and D_F) along with an error $E_C(\mu_a)$ (which is also the sum of squared residuals between actual values of contrast and their fitted values). Note that the errors E_I and E_C are μ_a dependent and are calculated for values of μ_a in a tissue-relevant interval.

Fig. 2 shows the error curves corresponding to the fit of the intensity and contrast profiles, E_I and E_C , as a function of μ_a . Both E_I and E_C go through minimum values ($E_{I,min}$ and $E_{C,min}$) corresponding to different μ_a values. The minimum of each error is pointed out in **Fig. 2** with the black dotted lines. $E_{C,min}$ and $E_{I,min}$ each correspond to a set of μ_a , μ'_s , τ_0 , τ_D , and D_F . The values for this specific simulated sample are presented in **Table 1**. The final estimated value of each of the 5 parameters of interest is taken as the average of its value estimated at $E_{I,min}$ and the one at $E_{C,min}$.

Table 1

Real and estimated parameters. The final estimated mean value corresponds to the average of the values estimated at E_{Imin} and E_{Cmin} for each parameter. Stdv% of final estimated corresponds to the standard deviation between the value estimated at E_{Imin} and the one estimated at E_{Cmin} . Stdv% of estimated vs real corresponds to the standard deviation between the final estimated mean value and the real value.

Optical and dynamical parameters	Real value	Value estimated at E_{Imin}	Value estimated at E_{Cmin}	Final estimated mean value	Stdv% of final estimated	Stdv% of estimated vs real
μ_a [cm^{-1}]	0.305	0.310	0.325	0.3175	3.3	2.8
μ'_s [cm^{-1}]	9.00	8.85	8.35	8.60	4.2	3.3
r_0 [cm]	$5.64\text{E-}7$	$5.73\text{E-}7$	$6.03\text{E-}7$	$5.88\text{E-}7$	3.5	2.8
τ_D [ms]	1.465	1.464	1.456	1.459	0.38	0.27
D_F [$\text{cm}^2\text{ms}^{-1}$]	$4.47\text{E-}14$	$4.64\text{E-}14$	$5.15\text{E-}14$	$4.89\text{E-}14$	7.0	6.1

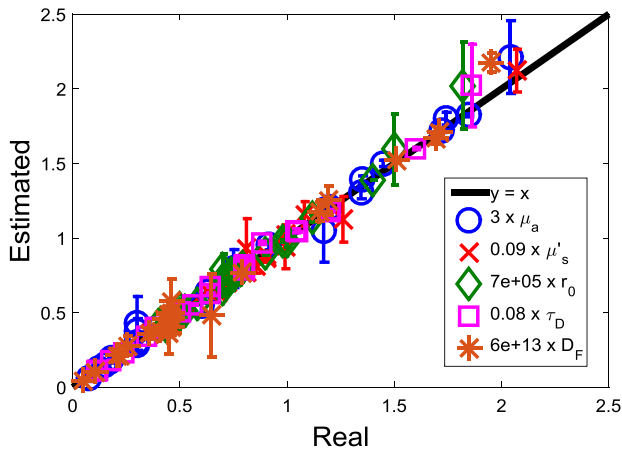


Fig. 3. Average fitted vs real parameters multiplied by different factors allowing their representation on the same graph.

Speckle images corresponding to numerous viscoelastic tissue-mimicking samples having different optical and dynamical properties, were simulated, and the fitting model was applied to the $I(r)$ and $C(r, T_{\text{exp}})$ curves in order to assess the estimation of μ_a , μ'_s , r_0 , τ_D , and D_F using the proposed methodology. The fitting procedure provides two optimal sets of parameters: one at E_{Cmin} , and one at E_{Imin} . Fig. 3 shows the average values over these two sets, with error bars corresponding to the standard deviation associated to this average, for 23 different simulated viscoelastic samples.

For all samples, the 5 parameters were accurately estimated. The relative error between real and estimated values ranges from 0.01 to 24% with a mean value of 3%. Furthermore, in most cases, this relative error is correlated to the standard deviation issued from the double estimation at E_{Cmin} and E_{Imin} . We therefore have here a criterion to assess the extracted parameters. In this range of precision, the proposed method could be well suited for numerous applications, where optical and dynamical characteristics are a key for diagnosing certain diseases [32,33] or for tracking different physiological changes in biological tissues [34].

2.3. Experimental application

In order to test the proposed approach on real biological media, experiments were performed on apple slices. We use the same experimental conditions as the ones described for the simulated media. A schematic view of the experimental setup is presented in Fig. 4. Speckle images of the scattering spot are acquired using a Hamamatsu (C8484-05G01) CCD camera with an objective of numerical aperture $NA = 0.045$. This value is close to the diffraction angle λ/a (where a is the pixel size of the camera): in fact, it corresponds to about 40% of the diffraction angle, in order to keep a reasonable value for β . This low NA value induces of course a sharp filtering on light directions, but this is not an issue in the multiple scattering regime where light direction quickly decorrelates [35]. The β factor was estimated from

Table 2

Estimated parameters for the tested apple slice.

Optical and Dynamical parameters	Value estimated at E_{Imin}	Value estimated at E_{Cmin}	Stdv% of final estimated
μ_a [cm^{-1}]	0.325	0.320	1.1
μ'_s [cm^{-1}]	7.531	7.670	1.3
r_0 [cm]	$5.17\text{E-}7$	$5.09\text{E-}7$	1.1
τ_D [ms]	1.548	1.566	0.81
D_F [$\text{cm}^2\text{ms}^{-1}$]	$3.63\text{E-}14$	$3.51\text{E-}14$	2.4

correlation measurements through both a calibrated solid medium and tracing paper, leading to the value $\beta = 0.54^2$. This value is consistent with the fact that we measure unpolarized light (factor 0.5 on β), and with the numerical aperture and the pixel size of our camera. To avoid saturation, the laser intensity is automatically adjusted in order to have the same mean speckle image intensity for all acquired images over the whole range of T_{exp} . The light source ($\lambda = 780$ nm) points directly to the apple's flesh (a slice of thickness $z = 1.2$ cm), far from its skin and seeds. $I(r)$ and $C(r, T_{\text{exp}})$ values are computed from the half of the scattering spot situated on the side that is opposite to the seeds in order to prevent collecting any photons that might have been scattered by those.

It has been well recognized that fruits exhibit viscoelastic behavior [36]. Their inner activity is often associated to the physical movement of cell walls and particles inside cells [37]. Therefore, in our theoretical fitting model, we use the same form of MSD, modeling confined and free diffusion. Fig. 5 shows the experimental $I(r)$ and $C(r, T_{\text{exp}})$ curves respectively, along with their theoretical fits, after extracting the optical and dynamical parameters using the approach described earlier (values reported in Table 2). We assumed typical values [38,39] for the refractive index and the anisotropy factor of $n = 1.4$ and $g = 0.8$. It is clear that the theoretical model, fitted using the extracted parameters, agrees well with the experimental results. When considering other forms of MSD, such as forms corresponding to exclusively confined or free diffusion, a lesser agreement between the experimental results and the fit is observed. Therefore, this preliminary experiment demonstrates the relevance of the hydrated viscoelastic regime to model the dynamics of scattering particles in apples. Furthermore, the fitted parameters estimated at E_{Cmin} and E_{Imin} are quite close, which gives confidence about the consistency of these results. The values obtained for μ_a and μ'_s are compatible with values previously reported for apples [38,40–43].

Additional work is however required to assess the accuracy of this methodology for real fruits. The method is indeed influenced by the anisotropy factor g and the refractive index n , taken as fixed parameters in the fitting process. It could therefore be important to have an accurate estimation of these parameters. Experiments should also be carried out on a significant number of apples for more representative results. Nevertheless, the fruit used in this study served as a means to illustrate the experimental methodology and to check the feasibility of the proposed approach on real biological tissues. The proposed method lays the groundwork for a promising technique to measure fruits optical and textural properties, that change with their maturation level or in case of a disease manifestation.

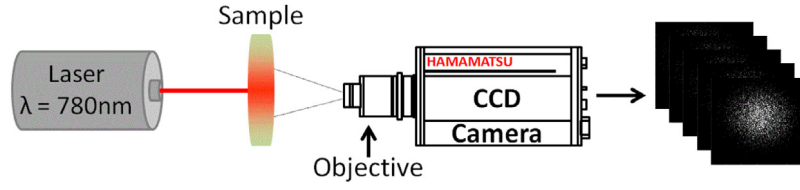


Fig. 4. Schematic view of the experimental setup. The images shown on the right, acquired by the CCD camera, are scattering spot images at different exposure times.

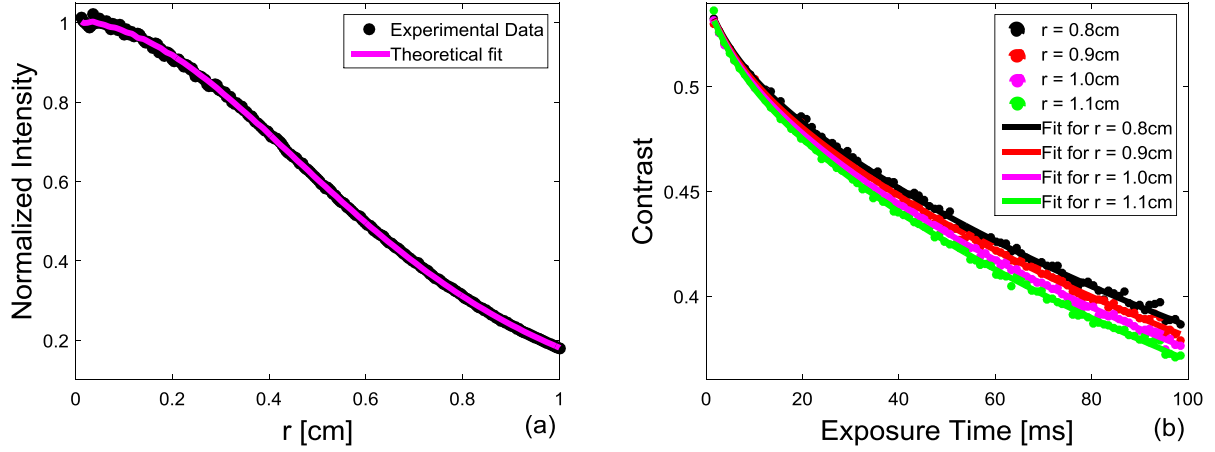


Fig. 5. Experimental data corresponding to measurements conducted on an apple slice (dots), fitted using the theoretical model with the estimated optical and dynamical parameters using the proposed approach (solid curves). Figure (a) shows the normalized intensity as a function of the radius r , and figure (b) shows the contrast C as a function of T_{exp} for different r radii with respect to the scattering spot center. With increasing r positions, a faster decay of the contrast is observed versus the exposure time.

3. Conclusion

In conclusion, using the proposed approach, it is possible to determine both optical and dynamical properties of viscoelastic media in a simple and non-contact manner. Further investigation should be performed on more apple tissues. Measurements of the optical properties of each tested apple must also be carried out using a conventional method, in order to quantify the exact errors on the assessment of the optical properties using the proposed approach. Moreover, information about the scattering particles size distribution in the sample should be gathered. This would allow the use of the generalized Stokes–Einstein relation [17–19] as mentioned previously, in order to be able to determine viscoelastic properties, namely the viscoelastic modulus $G^*(\omega)$, from the assessed dynamical parameters. The next step would be to adjust the proposed technique to backscattering geometry to allow non-invasive measurements directly in orchards. The study could also be extended to the case of non homogenous media, by simply performing contrast measurements only on selected homogeneous zones. Moreover, this method can be applied to various scattering media having different MSD types.

Acknowledgments

This study was financially supported by a grant (DIAGNOSIS) from Agence Nationale de la Recherche (ANR-15-CE21-0005).

Appendix

This appendix is devoted to the derivation of Eq. (1) from the reference [28]. Let us start with Eqs. (5), (6) and (7) from [28], respectively recalled hereafter:

$$g_2(\tau) = 1 + \frac{C_t(\tau)}{\langle I \rangle_t^2} \quad (\text{A.1})$$

$$g_2(\tau) = 1 + \beta |g_1(\tau)|^2 \quad (\text{A.2})$$

$$g_1(\tau) = \frac{\langle E(t)E^*(t+\tau) \rangle}{\langle E(t)E^*(t) \rangle} \quad (\text{A.3})$$

where $g_1(\tau)$ is the electric field temporal autocorrelation function, $g_2(\tau)$ is the intensity temporal autocorrelation function, and $C_t(\tau)$ is the temporal autocovariance of the intensity fluctuations in a single speckle grain. Using successively these three equations, one has:

$$\begin{aligned} C_t(\tau) &= \langle I \rangle^2 (g_2(\tau) - 1) = \beta \langle I \rangle^2 g_1^2(\tau) = \beta \langle I \rangle^2 \frac{\langle E(t)E^*(t+\tau) \rangle^2}{\langle E(t)E^*(t) \rangle^2} \\ &= \beta \langle I \rangle^2 \frac{G_1^2(\tau)}{G_1^2(0)} \end{aligned} \quad (\text{A.4})$$

where $G_1(\tau) = \langle E(t)E^*(t+\tau) \rangle$. For the time-averaged intensity we replaced $\langle I \rangle_t^2$ by $\langle I \rangle^2$. We then report this expression of $C_t(\tau)$ in the following equation (3) from reference [28]:

$$\frac{\sigma_s^2(T_{\text{exp}})}{\langle I \rangle^2} = \frac{2}{T_{\text{exp}} \langle I \rangle^2} \int_0^{T_{\text{exp}}} \left(1 - \frac{\tau}{T_{\text{exp}}}\right) C_t(\tau) d\tau \quad (\text{A.5})$$

where $\frac{\sigma_s^2(T_{\text{exp}})}{\langle I \rangle^2}$ is the square of the contrast. This gives us:

$$\begin{aligned} \frac{\sigma_s^2(T_{\text{exp}})}{\langle I \rangle^2} &= \frac{2\beta \langle I \rangle^2}{T_{\text{exp}} \langle I \rangle^2} \int_0^{T_{\text{exp}}} \left(1 - \frac{\tau}{T_{\text{exp}}}\right) \frac{G_1^2(\tau)}{G_1^2(0)} d\tau \\ &= \frac{2\beta}{T_{\text{exp}}^2} \int_0^{T_{\text{exp}}} (T_{\text{exp}} - \tau) \frac{G_1^2(\tau)}{G_1^2(0)} d\tau, \end{aligned} \quad (\text{A.6})$$

leading to the contrast given in Eq. (1) of this paper:

$$C(r, T_{\text{exp}}) = \frac{\sigma_s(T_{\text{exp}})}{\langle I \rangle} = \frac{1}{T_{\text{exp}}} \sqrt{2\beta \int_0^{T_{\text{exp}}} (T_{\text{exp}} - \tau) \frac{G_1^2(r, \tau)}{G_1^2(r, 0)} d\tau} \quad (\text{A.7})$$

where r illustrates the dependence on the distance from the scattering spot center.

References

- [1] M. Ahearne, Y. Yang, A.J. El Haj, K.Y. Then, K.K. Liu, Characterizing the viscoelastic properties of thin hydrogel-based constructs for tissue engineering applications, *J. R. Soc. Interface* 2 (2005) 455–463.
- [2] S. Aubry, J.R. Risson, A. Kastler, B. Barbier-Brion, G. Siliman, M. Runge, B. Kastler, Biomechanical properties of the calcaneal tendon in vivo assessed by transient shear wave elastography, *Skeletal Radiol.* 42 (2013) 1143–1150.
- [3] G. Tabilo-Munizaga, G.V. Barbosa-Canovas, Rheology for the food industry, *J. Food Eng.* 67 (2005) 147–156.
- [4] J.M. Mansour, D.W. Marine Gu, C.Y. Chung, J. Heebner, J. Althans, S. Abdalian, M.D. Schluchter, Y. Liu, J.F. Welter, Towards the feasibility of using ultrasound to determine mechanical properties of tissues in a bioreactor, *Ann. Biomed. Eng.* 42 (2014) 2190–2202.
- [5] S.P. Kearney, A. Khan, Z. Dai, T.J. Royston, Dynamic viscoelastic models of human skin using optical elastography, *Phys. Med. Biol.* 60 (2015) 6975–6990.
- [6] D. Preece, R. Warren, R.M.L. Evans, G.M. Gibson, M.J. Padgett, J.M. Cooper, M. Tassieri, Optical tweezers: wideband microrheology, *J. Opt.* 13 (2011) 044022–044028.
- [7] Z. Hajjarian, S.K. Nadkarni, Correction of optical absorption and scattering variations in laser speckle rheology measurements, *Opt. Express* 22 (2014) 6349–6361.
- [8] C.P. Valdes, H.M. Varma, A.K. Kristoffersen, T. Dragojevic, J.P. Culver, T. Durduran, Speckle contrast optical spectroscopy, a non-invasive, diffuse optical method for measuring microvascular blood flow in tissue, *Biomed. Opt. Express* 5 (2014) 2769–2784.
- [9] T.J. Farrell, M.S. Patterson, B. Wilson, A diffusion theory model of spatially resolved, steady-state diffuse reflectance for the noninvasive determination of tissue optical properties in vivo, *Med. Phys.* 19 (1992) 879–888.
- [10] P. Farzam, T. Durduran, Multidistance diffuse correlation spectroscopy for simultaneous estimation of blood flow index and optical properties, *J. Biomed. Opt.* 20 (2015) 55001.
- [11] D. Tamborini, P. Farzam, B. Zimmermann, K.C. Wu, D.A. Boas, M.A. Franceschini, Development and characterization of multidistance and multiwavelength diffuse correlation spectroscopy system, *Neurophotonics* 5 (2018) 011015.
- [12] M.Z. Ansari, L.C. Da Silva, J.V.P. Da Silva, A.M. Deana, Modelling laser speckle photographs of decayed teeth by applying a digital image information technique, *Laser Phys.* 26 (2016) 095602–095606.
- [13] N. Curry, P. Bondareff, M. Leclercq, N.F. Van Hulst, R. Sapienza, S. Gigan, S. Grésillon, Direct determination of diffusion properties of random media from speckle contrast, *Opt. Lett.* 36 (2011) 3332–3334.
- [14] C. Abou Nader, F. Pellen, P. Roquefort, T. Aubry, B. Le Jeune, G. Le Brun, M. Abboud, Evaluation of low viscosity variations in fluids using temporal and spatial analysis of the speckle pattern, *Opt. Lett.* 41 (2016) 2521–2524.
- [15] U. Tricoli, C.M. Macdonald, T. Durduran, A. Da Silva, V.A. Markel, Diffuse correlation tomography in the transport regime: a theoretical study of the sensitivity to brownian motion, *Phys. Rev. E* 97 (2018) 022408.
- [16] J. Wang, M. Hosoda, D.M. Tshikudi, Z. Hajjarian, S.K. Nadkarni, Intraluminal laser speckle rheology using an omni-directional viewing catheter, *Biomed. Opt. Express* 8 (2017) 137–150.
- [17] T.G. Mason, Estimating the viscoelastic moduli of complex fluids using the generalized Stokes-Einstein equation, *Rheol. Acta* 39 (2000) 371–378.
- [18] T.G. Mason, D.A. Weitz, Optical measurements of frequency-dependant linear viscoelastic moduli of complex fluids, *Phys. Rev. Lett.* 74 (1995) 1250–1253.
- [19] J.J. Duffy, C.A. Rega, R. Jack, S. Amin, An algebraic approach for determining viscoelastic moduli from creep compliance through application of the generalized Stokes-Einstein relation and burgers model, *Appl. Rheol.* 26 (2016) 15130–15136.
- [20] A.V. Teixeira, E. Geissler, P. Licinio, Dynamic scaling of polymer gels comprising nanoparticles, *J. Phys. Chem. B* 111 (2007) 340–344.
- [21] D. Chicea, S.M. Rei, A fast artificial neural network approach for dynamic light scattering time series processing, *Meas. Sci. Technol.* 29 (2018) 105201–105216.
- [22] E. Sarmiento-Gomez, I. Santamaria-Holek, R. Castillo, Mean-square displacement of particles in slightly interconnected polymer networks, *J. Phys. Chem. B* 118 (2014) 1146–1158.
- [23] B.J. Ackerson, R.L. Dougherty, N.M. Reguigui, U. Nobbmann, Correlation transfer: application of radiative transfer solution methods to photon correlation problems, *J. Thermophys. Heat Transfer* 6 (1992) 577–588.
- [24] R.L. Dougherty, B.J. Ackerson, N.M. Reguigui, F. Dorri-Nowkooari, U. Nobbmann, Correlation transfer: development and application, *J. Quant. Spectrosc. Radiat. Transf.* 52 (1994) 713–727.
- [25] D.A. Boas, L.E. Campbell, A.G. Yodh, Scattering and imaging with diffusing temporal field correlations, *Phys. Rev. Lett.* 75 (1995) 1855–1858.
- [26] D.A. Boas, I.V. Meglinsky, L. Zernany, L.E. Campbell, B. Chance, Diffusion of temporal field correlation with selected applications, in coherence-domain methods in biomedical optics, *Proc. SPIE* 2732 (1996).
- [27] U. Sunar, H. Quon, T. Durduran, J. Zhang, J. Du, C. Zhou, G. Yu, R. Choe, A. Kilger, R. Lustig, L. Loevner, S. Nioka, B. Chance, A.G. Yodh, Non-invasive diffuse optical measurement of blood flow and blood oxygenation for monitoring radiation therapy in patients with head and neck tumors, *J. Biomed. Opt.* 11 (2006) 064021–064034.
- [28] D.A. Boas, A.K. Dunn, Laser speckle contrast imaging in biomedical optics, *J. Biomed. Opt.* 15 (2010) 011109–011121.
- [29] L. Gmachowski, Fractal model of anomalous diffusion, *Eur. Biophys. J.* 44 (2015) 613–621.
- [30] N. Monnier, S.M. Guo, M. Mori, J. He, P. Lénart, M. Bathe, Bayesian approach to msd-based analysis of particle motion in live cells, *Biophys. J.* 103 (2012) 616–626.
- [31] L.G. Henyey, J.L. Greenstein, Diffuse radiation in the galaxy, *Astrophys. J.* 93 (1941) 70–83.
- [32] A. Gracia-Urbe, E.B. Smith, J. Zou, M. Duvic, V. Prieto, L.V. Wang, In-vivo characterization of optical properties of pigmented skin lesions including melanoma using oblique incidence diffuse reflectance spectroscopy, *J. Biomed. Opt.* 16 (2011) 020501–020504.
- [33] B.J. Tromberg, N. Shah, R. Lanning, A. Cerussi, J. Espinoza, T. Pham, L. Svaasand, J. Butler, Non-invasive in vivo characterization of breast tumors using photon migration spectroscopy, *Neoplasia* 2 (2000) 26–40.
- [34] Y. Shi, L. Jiang, L. Zhang, R. Kang, Z. Yu, Dynamic changes in proteins during apple (*malus x domestica*) fruit ripening and storage, *Horticulture Res.* 1 (2014) 6.
- [35] L. Pattelli, R. Savo, M. Burreli, D.S. Wiersma, Spatio-temporal visualization of light transport in complex photonic structures, *Light Sci. Appl.* 5 (2016) e16090.
- [36] P. Varela, A. Salvador, S. Fiszman, Changes in apple tissue with storage time: rheological, textural and microstructural analyses, *J. Food Eng.* 78 (2007) 622–629.
- [37] A. Zdunek, A. Adamiak, P.M. Pieczywek, A. Kurenda, The biospeckle method for the investigation of agricultural crops: a review, *Opt. Lasers Eng.* 52 (2014) 276–285.
- [38] M.L. Askoura, F. Vaudelle, J.P. L'Huillier, Numerical study of light transport in apple models based on Monte Carlo simulations, *Photonics* 3 (2016).
- [39] L. Baranyai, M. Zude, Analysis of laser light migration in apple tissue by Monte Carlo simulation, *Progr. Agr. Eng. Sci.* 4 (2018) 45–59.
- [40] M.L. Askoura, F. Vaudelle, J.P. L'Huillier, Experimental study of light propagation in apple tissues using a multispectral imaging system, *Photonics* 3 (2016).
- [41] P.I. Rowe, R. Kunemeyer, A. McGlone, S. Talele, P. Martinsen, R. Seelye, Relationship between tissue firmness and optical properties of royal gala apples from 400 to 1050 nm, *Postharvest Biol. Technol.* 94 (2014) 89–96.
- [42] W. Saeys, M.A. Velazco-Roa, S.N. Thennadil, H. Ramon, B.M. Nicolai, Optical properties of apple skin and flesh in the wavelength range from 350 to 2200 nm, *Appl. Opt.* 47 (2008) 908–919.
- [43] R. Lu, H. Cen, M. Huang, D.P. Ariana, Spectral absorption and scattering properties of normal and bruised apple tissue, *Trans. ASABE* 53 (2010) 263–269.